Flexible operation of large-scale coal-fired power plant integrated with solvent-based post-combustion CO_2 capture based on neural network inverse control

Peizhi Liao[a], Yiguo Li[a, *], Xiao Wu[a, *], Meihong Wang[b], Eni Oko[b]

[a]Key laboratory of Energy Thermal Conversion and Control of Ministry of Education , Southeast University, Nanjing 210096, China
[b]Department of Chemical and Biological Engineering, University of Sheffield, Sheffield S1 3JD, UK

Abstract

Post-combustion carbon capture (PCC) with chemical absorption has strong interactions with coal-fired power plant (CFPP). It is necessary to investigate dynamic characteristics of the integrated CFPP-PCC system to gain knowledge for flexible operation. It has been demonstrated that the integrated system exhibits large time inertial and this will incur additional challenge for controller design. Conventional PID controller cannot effectively control CFPP-PCC process. To overcome these barriers, this paper presents an improved neural network inverse control (NNIC) which can quickly operate the integrated system and handle with large time constant. Neural network (NN) is used to approximate inverse dynamic relationships of integrated CFPP-PCC system. The NN inverse model uses setpoints as model inputs and gets predictions of manipulated variables. The predicted manipulated variables are then introduced as feed-forward signals. In order to eliminate steady-state bias and to operate the integrated CFPP-PCC under different working conditions, improvements have been achieved with the addition of PID compensator. The improved NNIC is evaluated in a large-scale supercritical CFPP-PCC plant which is implemented in gCCS toolkit. Case studies are carried out considering variations in power setpoint and capture level setpoint. Simulation results reveal that proposed NNIC can track setpoints quickly and exhibit satisfactory control performances.

Keywords: Post-combustion carbon capture; Coal-fired power plant; Dynamic modelling; Dynamic simulation; Neural network inverse control

1. Introduction

1.1 Background

Large-scale power unit from fossil-fuel combustion, such as coal, petroleum and natural gas, remains to be the largest source of carbon emission. Globally, around 65% of total electricity was provided by natural gas and coal-fired power plants in 2015 [1]. Compared with natural gas fired power plant, coal-fired power plants (CFPPs) emit the most amount of CO_2 per unit of electricity [2]. The resulting climate change has attracted world-wide attentions in recent years. It has been suggested to develop an effective CO_2 emission abatement strategy for large stationary source. With a strong motivation for the development and deployment of new carbon emission reduction technology, MEA-based post-combustion carbon capture (PCC) process is proven to be the most mature and economically appealing option [3]. It can be easily installed as an end-of-pipe solution with minimum modifications to the existing power plant configurations.

Carbon capture process has strong interactions with power plant. The responses of solvent-based PCC process to variations of upstream power generation plant have been demonstrated [4-5]. The interactions between different variables are very strong and the dynamics of the PCC and CFPP system exhibit large time constant. These features would present additional control challenges for the integrated CFPP-PCC system. Due to variations in electricity demand and increased installation of renewable energy sources, there will be associated need for CFPPs to be operated in load-following mode to satisfy grid demand at all time [6]. In this case, the flue gas flowrate will follow the load variation of CFPP and thereby influence downstream PCC process. This may deteriorate control performance or even lead to instability of the PCC control system. Another concern is the massive energy penalty would be incurred for solvent regeneration. The heat is provided by extracted steam from crossover pipe between the intermediate and low-pressure steam turbine. For a CFPP, it has been estimated that PCC process at end-of-pipe will reduce electricity output by around 15%, which is a major reason that limits worldwide commercial deployment of PCC technology [3]. The energy penalty would be even higher if the PCC process is not operated optimally.

Nomenclature

c	specific heat capacity (kJ/(kg·℃))	Greek symbols	
D	mass flowrate (kg/s)	ρ	density (kg/m^3)
h	specific enthalpy (kJ/kg)	τ	time delay in pulverizing system (s)
k_0	coal pulverizer time constant (s)	μ	throttle valve opening
k_1	heat absorption coefficient in furnace (kJ/kg)	η	efficiency of steam turbine (%)
k_2	steam turbine gain		
l	specific value of specific enthalpy	Subscripts	
M	mass (kg)	a	fluid (including water and vapor) in the boiler
N_e	Net power output (MW)	fw	feedwater flow
P	Pressure (MPa)	j	total metal in the boiler section
Q	heat absorption in boiler section (kJ)	m	steam flow at the outlet of separator
r_B	fuel mass flowrate to the boiler (kg/s)	s	steam flow at the outlet of superheater
$r_B^{'}$	fuel mass flowrate to the pulverizer (kg/s)	st	main steam flow
s_1	dynamic parameter of steam separator	sw	desuperheating water flow
s_2	dynamic parameter of steam separator		
T	temperature (℃)	Superscript	
u_B	fuel command flowrate (kg/s)	$*$	steady-state value
V_t	total volume of water and vapor in the boiler (m^3)		

In view of the aforementioned challenges, there is a strong need to enhance flexible controllability for PCC process. Nevertheless, PCC and CFPP has strong physical and energic interactions. Studies on individual PCC process are insufficient to operate the integrated CFPP-PCC system. As a result, it is necessary to consider the PCC and CFPP as an integrated system and to investigate transient behaviors of the whole system. There are several advantages to control the integrated CFPP-PCC system: i) in the face of electricity peak load, it requires to track grid setpoint quickly and smoothly. Carbon capture can be compromised to allow more steam for power generation; ii) with a strict requirement for carbon capture level, the integration of CFPP and PCC can be utilized. Coal mass flowrate can be reduced so that the decreasing flue gas flowrate can result in a higher carbon capture level. Feedforward control can be introduced to manipulated lean solvent flowrate and steam flowrate in advance based on a prediction of flue gas flowrate and iii) trade-off can be achieved to balance the operation for PCC and CFPP for an optimal control.

1.2 Previous studies

The current studies of solvent-based PCC process lie primarily on steady-state optimization, which mainly considers the effect of different solvents, configurations, operating parameters and techno-economic analysis [7-14]. Steady-state models are firstly developed to study its inherent nature [15-16]. However, steady-state models are unable to replicate transient behavior of actual PCC process and cannot provide enough information for controller design. Dynamic modelling based on two different approaches, namely, equilibrium approach and rate-based approach are therefore presented. Lawal et al [11] proved that rate-based approach gives more accurate results to predict temperature profile in absorber. Various simulation software has been used for modelling, including gCCS [4-6, 13], gPROMS® [10-12, 17], Aspen Plus® [7-9, 11-12, 18], Modelica [19-20] and Matlab [21-22]. PCC process has strong nonlinear features and large time inertial [2]. To overcome these challenges and to reinforce the controllability of PCC process, decentralized PID controllers [23-26] and advanced decentralized controllers, e.g. model predictive control (MPC) [6, 21, 27-29] and adaptive control [30] have been employed. The targets included in these studies can be summarized as: (a) Setpoints tracking and disturbance rejection; (b) Hydraulic stability; (C) Optimization on minimizing the overall cost under varying price scenarios [31]. Through simulation, it is found that MPC is capable of dealing with these issues and achieving better control performance. The main advantage of MPC over conventional PID controller is the ability to handle with constraints. It also enables the PCC system to be operated optimally. However, MPC is based on an explicit mathematical model to predict the future reactions of controlled variables [32]. This would increase model complexity and add additional computation time. Furthermore, any mismatch in mathematical model or disturbances will reduce MPC's reliability and deteriorate control performance. On the

contrary, PID controller has strong robustness and it is able to work under varying working conditions. Due to its inherent nature, PID controller is easy to implement and it is so far the most widely used control technique in industry. It can be expected that a conventional PID controller with improved technology would still be appealing in controlling PCC process.

Compared with studies in standalone PCC process, current researches for dynamic simulation and control of integrated CFPP-PCC process is still in an early stage. Most of them are still restricted to steady-state analysis in terms of net power efficiency and energy penalty. Aroonwilas and Veawab carried out steady-state simulation for a 500MW CFPP with a PCC process in terms of net thermal efficiency and CO_2 emission [33]. It is suggested to use a blended MEA-MDEA solvent and a split-flow rich solvent configuration to lower energy penalty. In Cifre et al [34], PCC process was simulated with the integration of a 600MW hard coal and a 1000MW lignite power station. The main purpose is to investigate the influences on reboiler duty and power plant efficiency under varying stripper operating pressure. Sanpasertparnich et al [35] proposed steady-state analysis under full and partial load. The results exhibit higher energy consumption for partial load scenario. The system performance in the face of different coal types and steam extraction locations were presented. Olaleye et al [36] presented a steady-state simulation and exergy analysis of PCC process integrated with a 550MW supercritical CFPP. Olaleye et al tested 4 configuration cases separately, namely, conventional PCC process, absorber intercooling (AIC), split-flow (SF), and a combination of AIC and SF. The last option presents the most significant reduction in energy penalty. Similarly, in Zhai et al [37], 3 integration methods were investigated for an integrated facility to a 660MW CFPP with NH_3-based PCC process. Steady-state analysis reveals that steam extraction from the IP/LP crossover pipe and the condensate returning to the deaerator contributes to the lowest efficiency loss. In order to minimize efficiency penalty for a 550MW CFPP retrofitted with PCC process, steady-state parametric optimization and configuration improvement were undertaken in Se-Young et al [38]. It is found that the energy consumption can be significantly reduced by the combination of structural modifications and by exploiting optimal steam extraction point.

The above studies are only steady-state analysis and do not consider the dynamic behaviors of the integrated system. As stated previously, the CFPP needs to participate in grid demand regulation and the PCC process is required to adapt with the variation in flue gas flowrate. Due to strong interactions between two systems, flexible operation has been expected to attain a satisfactory control performance. To this end, it is necessary to look into the dynamic characteristics of integrated CFPP-PCC system and design suitable control structure. Lawal et al [17] presented a dynamic PCC model integrated with CFPP to an industrial size of 500MW. This is the first paper regarding the dynamic simulation of the integrated system. Three main links are used for process integration: i) The flue gas stream from CFPP; ii) The steam draw-off from steam turbine for solvent regeneration; iii) The condensate return from reboiler to CFPP. The simulation reveals strong interaction between the two systems and the PCC process has a much larger time constant compared with that of CFPP. Tuning PI controller parameters is advised to achieve better control performance. Olaleye et al [39] operated a full-scale integrated system under UK grid demand. It is suggested that a stripper stop can be used to aid in primary response. The authors further showed that the stripper stop mechanism can achieve about 4.67% MCR increase in power generation. However, an in-depth investigation of stripper stop mechanism and available control structure are beyond the scope of current study. Wu et al [40] presented a centralized MPC in order to ensure a flexible operation of an integrated CFPP-PCC system. Interactions between multi-variables can be utilized to make a trade-off between CFPP and PCC process. Two independent MPCs with the same sampling time and conventional PI controllers were set as comparison. Three operation cases were tested respectively: i) rapid power tracking mode; ii) strict carbon capture mode and iii) normal operation mode. It is found that independent MPCs cannot utilize the interactions between two systems. A centralized MPC for integrated system is important for the operation of CFPP-PCC unit. In his follow-up work [41], a reinforced coordinated control structure is presented to make a better use of the interactions between CFPP and PCC process. The flue gas flowrate and steam flowrate are introduced as additional feedforward signals. The estimation of feedforward signals can be fully utilized by each sub-MPC to better coordinate the operation of PCC and CFPP system. The simulation results show that the presented coordinated controller has a better performance compared with independent MPCs and conventional PI controllers. However, the CFPP-PCC model in Wu' work is at a pilot scale (0.25MW) as such cannot fully represent the actual features of large-scale CFPP-PCC process.

The limitation of aforementioned studies is lack of in-depth research into the large-scale CFPP-PCC process. As a result, it cannot provide reliable information for flexible operation in real industry. It is necessary to develop a large-scale CFPP model integrated with PCC process and assess transient behaviors. In addition, advanced control structures should be developed based on the dynamic characteristics of CFPP-PCC process in order to improve the control performance

1.3 Novel contributions

The objective of this paper is to develop a dynamic model for a large-scale CFPP-PCC system with a concurrent improved neural network inverse control in order to improve control performance. There are two major novelties:

- Analysis of dynamic characteristics for a large-scale integrated CFPP-PCC process;
- An improved neural network inverse control is introduced with the combination of PID compensator.

In this paper, the dynamic interactions among different variables within a large-scale CFPP-PCC process are investigated. This information will contribute to controller design for the whole system. To operate the CFPP-PCC process in a flexible manner, an improved neural network inverse control (NNIC) is presented. The NNIC structure has been applied in many different areas due to its appealing advantages [42-44]. NNIC considers the interactions of different variables which makes it appropriate for multi-input-multi-output system. In addition, neural network is able to precisely model the inverse dynamic relationships of controlled system and this enables NNIC to be utilized as a feedforward controller. Based on the standalone NNIC proposed in [42-44], this paper presented an improved NNIC with an additional PID compensator in order to eliminate prediction error of neural network inverse model. Given this context, the improved NNIC is able to achieve a feedforward adjustment on the manipulated variables. It can therefore adjust the net power output and CO_2 capture level reaching targets quickly. Meanwhile, it can lower the fluctuations in other crucial controlled variables like steam pressure, steam enthalpy and reboiler temperature.

1.4 Outline of current paper

The scope of the current study is set up as follows: Section 2 presents the system description of the integrated CFPP-PCC process, including model development of CFPP, PCC system and the process integration. Section 3 details the proposed neural network inverse control structure. The dynamic characteristics of CFPP-PCC process are investigated in Section 4. Simulations are carried out in Section 5. Conclusions are drawn in Section 6.

2. System description of integrated CFPP-PCC system

To investigate the dynamic characteristics of the CFPP-PCC plant, a large-scale super-critical CFPP model and MEA-based PCC model are presented in this section. The super-critical CFPP model is successfully validated using operational data from a 660MW supercritical CFPP unit. The CFPP-PCC model is implemented in gCCS modelling environment.

2.1 Model development of CFPP

In order to reduce modelling complexity and computational load, only the main sections of CFPP are considered which include: coal pulverizing system, boiler section and steam turbine section. In CFPP system, coal pulverizer takes a long time (5-15 minutes) to grind coal before sending them to furnace. It contributes to major time delay to the characteristics of the CFPP system. The boiler and steam turbine section are main components of a power plant. It is of great importance to consider these units in model development. To maintain the balance between model accuracy and simplicity, several assumptions are made as follows [44]:

a) Lumped parameter modelling approach;
b) The composition and quality of feed coal keep the same;
c) There is no steam and energy loss in the system;
d) Heat absorption along the water fall is evenly distributed;
e) Water wall, economizer and superheater can be regarded as a heated pipe with same volume;
f) Properties of vapour stream is evenly distributed at any cross section of the heated pipe.

2.1.1 Coal Pulverizing system

Raw coal needs to be pulverized in a coal mill before being supplied to furnace. A direct-fired pulverizing system is obtained in the current section. The pulverizing process and the transportation of pulverized coal contributes to major time delay in pulverizing system. The time delay, which is mainly due to slow response in the primary air tube and the coal feeder, can be expressed as

$$r_B^{'} = u_B e^{-\tau s} \tag{2}$$

The overall mass balance in the coal mill is given in Eq. (2)

$$\frac{dM}{dt} = r_B^{'} - r_B \tag{3}$$

where M can be expressed as $M = k_0 r_B$ according to the dynamic features in coal mill [46]. k_0 is related to the property of coal mill and it is regarded as a constant.

2.1.2 Boiler section

Heat generated in furnace is then transferred to water walls, superheaters, reheaters and economizers [17]. Based on the assumptions presented in Section 2.1, these units can be regarded as heated pipes. The mass balance and the energy balance for the steam side in boiler section can be shown in Eqs. (3-4)

$$V_t \frac{d\rho_a}{d_t} = D_{fw} - D_s \tag{4}$$

$$V_t \frac{d\rho_a h_a}{d_t} + c_j m_j \frac{dT_j}{dt} = D_{fw} h_{fw} - D_s h_s + Q \tag{5}$$

Given the fact that coal combustion in furnace has a much smaller time constant compared to that of a whole CFPP. It is therefore taken that the heat absorption Q is proportional to the coal mass flowrate [47].

$$Q = k_1 r_B \tag{6}$$

Remark. $V_t(d\rho_a h_a/d_t)$ denotes the variation of energy stored in the steam side, including unsaturated water, saturated water, saturated steam, and superheated steam. The term $c_j m_j(dT_j/d_t)$ represents the variation of energy stored in the pipe metal based on the assumption that water wall, economizer and superheater are regarded as a heated pipe. It is necessary to consider the metal energy storage in the boiler to improve model accuracy.

The modelling of super-critical CFPP is different with the modelling of sub-critical CFPP. In a sub-critical CFPP, the steam drum behaves as a storage tank with water and steam. It is a relatively independent unit and can dampen the fluctuation of feedwater flowrate. However, super-critical CFPP doesn't have steam drum. Feedwater absorbs heat and turns into steam directly. As a result, feedwater flowrate has a strong impact on main steam pressure and net power output. To maintain the process, it is necessary to control the coal-feedwater ratio to a certain level. The specific enthalpy of steam in the outlet separator is very sensitive to coal-feedwater ratio and the corresponding pressure and temperature of steam in outlet separator are measurable. Hence the state parameters of steam in the outlet separator can be used to replace the fluid parameter (h_a, ρ_a) in Eqs. (3-4). The dynamic mass and energy balance equations in the separator is given as

$$s_1 \frac{d\rho_m}{d_t} = D_{fw} - D_s \tag{7}$$

$$s_2 \frac{d\rho_m h_m}{d_t} + c_j m_j \frac{dT_j}{dt} = D_{fw} h_{fw} - lD_s h_m + Q \tag{8}$$

where $l = \frac{h_{st}}{h_m}$.

In general, ρ_m is assumed to be a function of separator's temperature and pressure. Partial derivatives are calculated with respect to p_m and h_m. Eqs (6) and (7) are rewritten as

$$b_{11}\frac{dp_m}{dt}+b_{11}\frac{dh_m}{dt}=D_{fw}-D_s \tag{9}$$

$$b_{21}\frac{dp_m}{dt}+b_{22}\frac{dh_m}{dt}=D_{fw}h_w-lD_sh_m+Q \tag{10}$$

where $b_{11}=s_1\frac{\partial\rho_m}{\partial p_m}$, $b_{11}=s_1\frac{\partial\rho_m}{\partial p_m}$, $b_{21}=s_2h_m\frac{\partial\rho_m}{\partial p_m}+c_jm_j\frac{\partial T_j}{\partial p_m}$, $b_{22}=s_2(h_m\frac{\partial\rho_m}{\partial p_m}+\rho_m)+c_jm_j\frac{\partial T_j}{\partial p_m}$

The attemperator model is obtained to maintain a desired main steam temperature. In comparison with the time constant for the CFPP, the internal dynamics of the attemperator are extremely small. As a result, steady-state Eqs. (10) and (11) are used to describe the mass and energy balance of the attemperators.

$$D_s+D_{sw}=D_{st} \tag{11}$$

$$lD_sh_m+D_{sw}h_{sw}=D_{st}h_{st} \tag{12}$$

2.1.3 Steam Turbine section

The flowrate of superheated steam is related with its thermophysical parameters and steam turbine valve position. It can be represented by Eq. (12) [48].

$$D_{st}=\lambda\mu_t p_{st}^{1-\alpha}\rho_{st}^{\alpha} \tag{13}$$

where λ and α are fitting parameters. α is related to steam state. It ranges from 0 to 0.5, where α=0 is for a saturated steam flow and α=0.5 for ideal superheated steam flow.

Given the fact that the turbine section and the regenerative system have a much faster response, a zero-order steady-state model can be used to describe power generation, as shown in Eq. (13).

$$Ne=k_2D_{st}(h_{st}-h_{fw}) \tag{14}$$

2.2 Parameter identification of CFPP and model validation

With the development of first-principle CFPP model, parameters of these equations can be obtained through system identification. In this section, identification data is from the operational data base of a 660MW super-critical CFPP. The sampling interval is 10s. A particle swarm optimization (PSO) algorithm is used for identification. Recently, PSO algorithm has become an appealing technique for system optimization due to its simple concept and easy implementation. It has the advantages of less computational complexity and quick convergence over other intelligence algorithms [49]. In this paper, parameters' estimation for the CFPP can be viewed as a multi-dimensional optimization problem [50], which makes the utilization of PSO algorithm possible.

The optimization procedure is graphically explained in Fig. 1. The first step is to specify key parameters for PSO algorithm including solution limitation, population size and maximum iteration number. Thereafter, the random velocity and position for each particle are initialized. The total numbers of particles are the numbers of CFPP parameters to be estimated. The position of each particle is the exact value for each parameter and the velocity denotes the rate of change for each particle. After initialization, the fitness of each particle is calculated using Eq. (14)

$$fitness=\sum_{i=1}^{n}\left(\left(\frac{\Delta p_{st}}{p_{st}^*}\right)^2+\left(\frac{\Delta p_m}{p_m^*}\right)^2+\left(\frac{\Delta N_e}{N_e^*}\right)^2+\left(\frac{\Delta r_B}{r_B^*}\right)^2+\left(\frac{\Delta h_m}{h_m^*}\right)^2\right) \tag{15}$$

where Δ denotes the deviation between simulated result and measured data.

In every iteration, the best fitness achieved in current swarm and the corresponding position are recorded. This is called individual best. Another best value obtained by any particle over time (in current and previous iteration) is also tracked. This best value is a global best. With these two best values, particles' velocity and particles' position can be updated using Eqs. (15) and

(16)

$$v_{k+1}^{i} = \varphi v_{k}^{i} + \varsigma_1 rand(p_{k}^{i} - x_{k}^{i}) + \varsigma_2 rand(p^{g} - x_{k}^{i}) \tag{16}$$

$$x_{k+1}^{i} = x_{k}^{i} + v_{k+1}^{i} \tag{17}$$

where v denotes velocity and x represents position. φ, ς_1, ς_2 denote inertia factor, self-confidence factor and swarm confidence factor respectively. The superscript i is for the i^{th} particle and the subscript k is for the k^{th} iteration. The p_k^i is the individual best value of the i^{th} particle and p^g is the global best value.

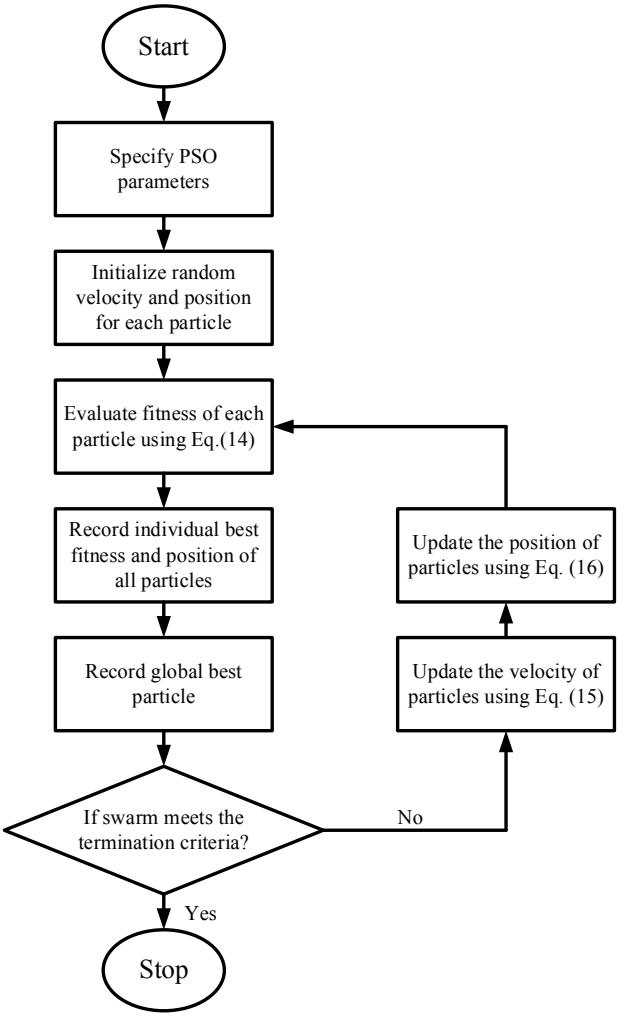

Fig. 1 Flowchart of PSO training procedure.

When maximum iterations or minimum fitness value are achieved, the PSO algorithm stops training. If it doesn't satisfy termination criteria, position and velocity of each particle are updated and then go back to fitness calculating step. Going through PSO identification, the major static and dynamic parameters of CFPP model are listed in Table 1.

Table 1. Identified parameters of CFPP model

Identified Parameters	Values
l	1.2846
k_0	89
k_1	15584.8
k_2	0.00054874
τ	27.35

The dynamic validation is then carried out to evaluate the effectiveness of the developed super-critical CFPP model. Validation data comes from the operational data base from a 660MW supercritical CFPP unit. The power output ranges from 400MW to 530MW. Comparison between simulation results and measured data are shown in Figs. 2-4. It is clear that the proposed model is able to capture the dynamics of the CFPP over a wide load range. The proposed model can predict the main steam pressure, steam enthalpy and power output with reasonable agreement around the operating points. However, the predictions of the main steam pressure and the steam enthalpy exhibit larger deviation towards the end of simulation.

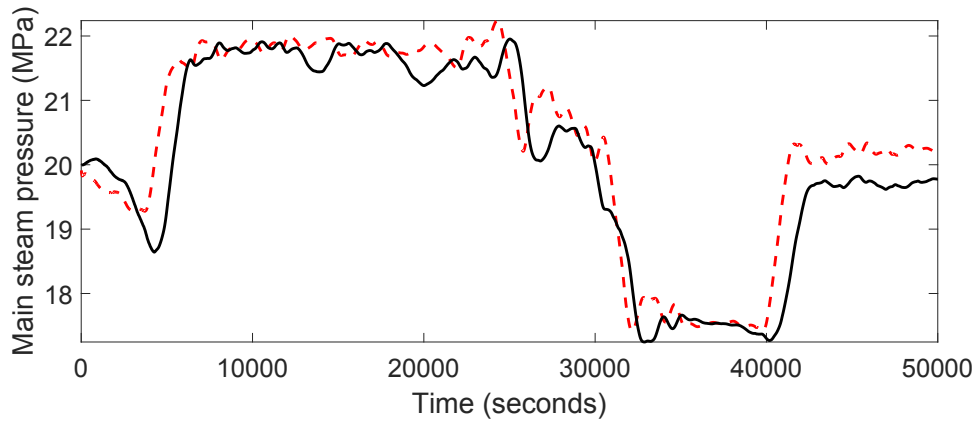

Fig. 2 Validation on main steam pressure (solid in black: measured data; dashed in red: simulation result).

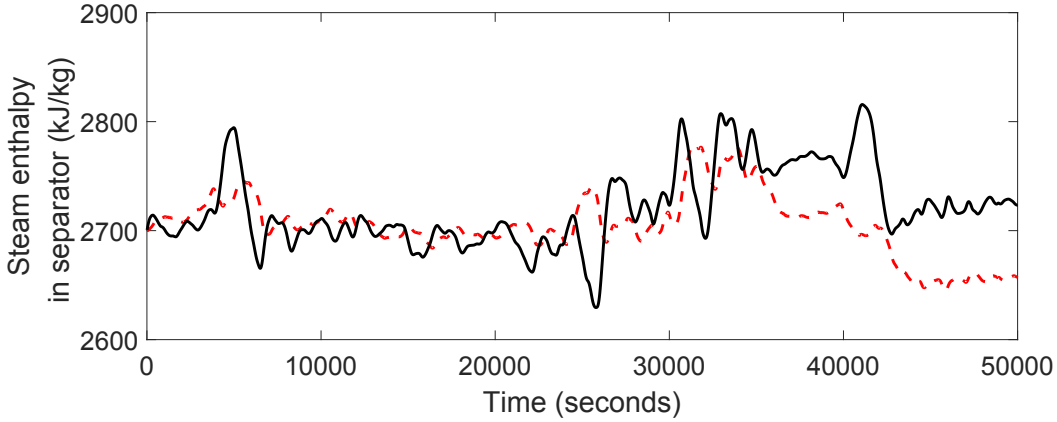

Fig. 3 Validation on steam enthalpy in separator (solid in black: measured data; dashed in red: simulation result).

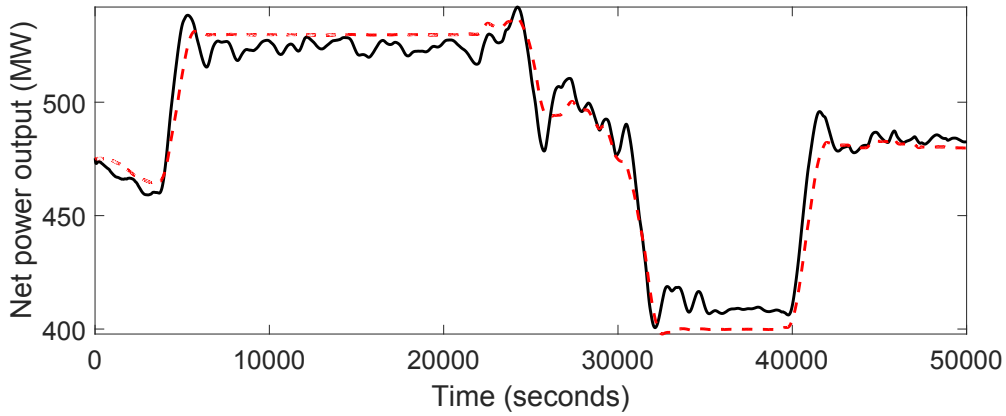

Fig. 4 Validation on net power output (solid in black: measured data; dashed in red: simulation result).

2.3 Scale up of the PCC model

The PCC dynamic model is originally based on a pilot-scale reference model in Lawal et al [11]. To adapt with the flue gas from a 660MW CFPP, this model is scaled up using the generalized pressure drop principle in [51]. A 42 mm water per meter of packing height pressure drop is assumed for both the absorber and the stripper. The flue gas flowrate from the power plant at full load is 600kg/s with a CO_2 wt% of 21.5%. The estimated solvent flowrate for achieving 90% capture level is around 2840 kg/s using 30 wt% MEA as absorption solvent.

From scale-up calculations, the absorber and stripper specifications shown in Table 2 can be obtained. The detailed scale-up methodology is available in Lawal [52]. The choice of more than one absorber is to help improve turndown ratio of PCC process and to reduce structure size of a single column [17]. In addition, it will have a better liquid and gas distribution allowing the PCC process to be operated in a more flexible manner. However, it is not possible to validate the industrial-size PCC model due to lack of operating data at this scale. The PCC model has been validated at pilot scale in Lawal et al [11].

Table 2. Design parameters from PCC scale up

Description	Absorber	Stripper
Column numbers	3	1
Packing type	IMTP 50	Mellapak 250Y
Specific area (m^2/m^3)	145	250
Height (m)	20	22
Diameter (m)	13	17
Operating pressure (bar)	1.01	1.8
Capture level (%)	90	/

2.4 Process integration of the super-critical CFPP and the PCC model

For system integration, three major links from Lawal et al [17] are used between the PCC and the CFPP, which include:

- The flue gas stream is pretreated (SO_x, NO_x and particulate removal and cooling to 40℃) and then sent to the bottom of absorber;
- The steam from the cross-over piper between the high-pressure and the intermediate pressure turbine is extracted at saturated state and then sent to reboiler;
- The condensate from the bottom of reboiler is returned to the power plant deaerator.

The schematic topology of integrated CFPP-PCC process is presented in Fig. 5. The flue gas is split equally into 3 parts, each part respectively entering the 3 absorbers. The lean solvent is similarly divided and then pumped to the top of 3 absorbers. It is expected that these 3 absorbers are in the same state at any time. The rich solvent streams from the bottom of 3 absorbers are then fully mixed before entering the cross-heat exchanger. The nominal operating values of some key variables for the integrated CFPP-PCC model are displayed in Table 3.

Table 3. Nominal operating values of key variables for integrated CFPP-PCC model

CFPP Variables	Value	PCC variables	Value
Coal mass flowrate (kg/s)	56.5333	Lean solvent flowrate (kg/s). [a]	497.680
Feedwater flowrate (kg/s)	397.630	Capture level (%)	90
Main steam valve position (%)	86.31	MEA concentration (wt%)	30
Main steam pressure (MPa)	21.3693	Absorber pressure (bar)	1.01
Steam enthalpy in separator (kJ/kg)	2722.1325	Steam flowrate (kg/s)	131.506
Net power output (MW)	432.9270	Reboiler pressure (bar)	1.8
Flue gas flowrate (kg/s)	483.3539	Reboiler temperature (K)	392.2

[a] The lean solvent flowrate refers to the lean solvent after division. The total mass flowrate is 3 times the value.

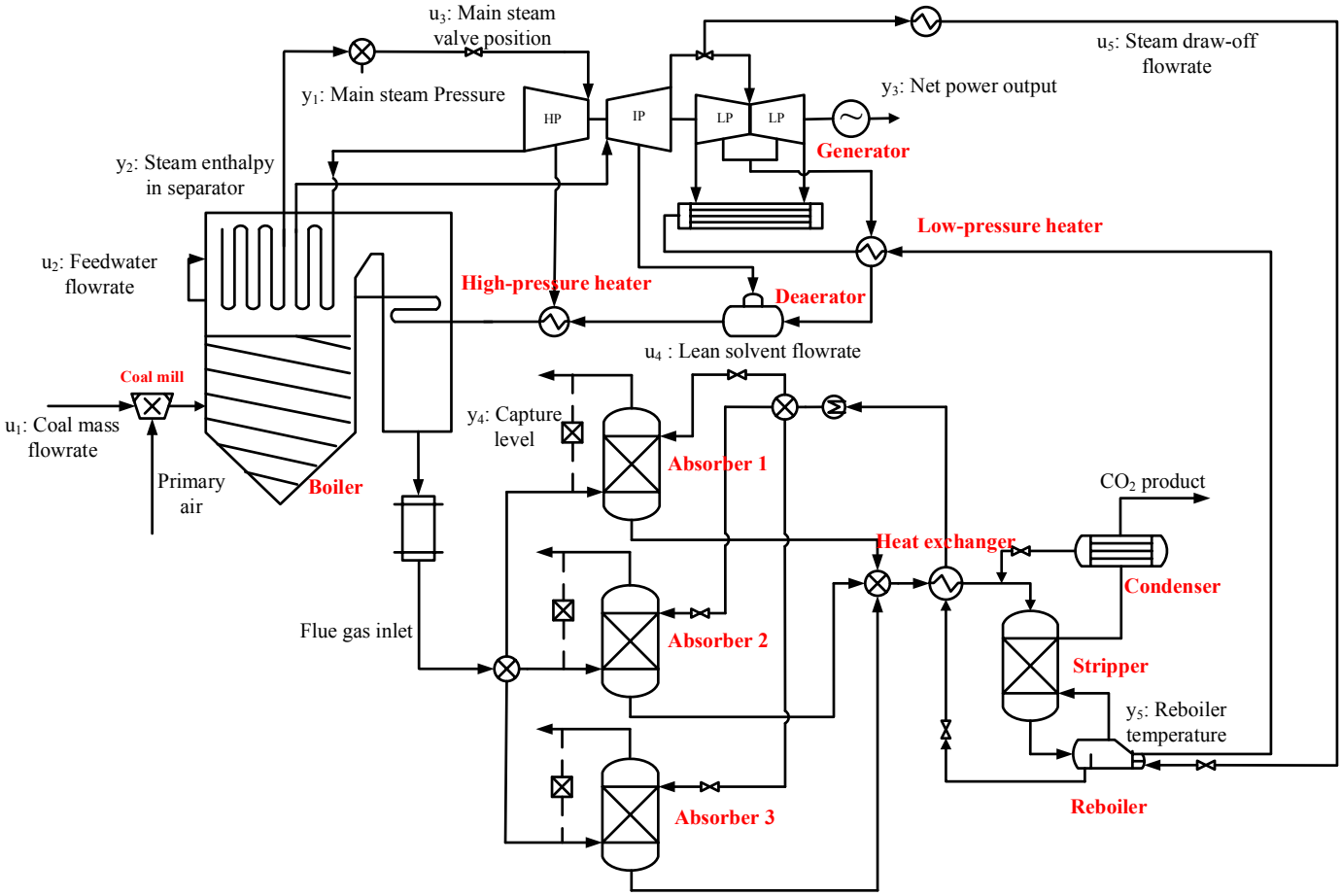

Fig. 5 Schematic topology of integrated CFPP-PCC process

Remark. It should be noted that the flue gas flowrate in Table 3 refers to the total mass flowrate before it is divided into 3 equal parts, as presented in Fig. 5. For simplicity, the lean solvent flowrate and MEA concentration refer to the inlet lean solvent properties after division. The total mass flowrate is 3 times the value listed in Table 3 while MEA concentration value is the same. The capture level and the absorber pressure of absorber 1 are listed as example. Meanwhile, all the 3 absorber parameters have the same capture level and absorber pressure. Through steady-state optimization, 392.2 K was obtained as the optimal operating temperature for the reboiler at the pressure of 1.8 bar. In current reboiler temperature, PCC process has the minimum reboiler duty. To save space, the details of steady-state optimization are not presented in the proposed manuscript.

3. Neural network inverse control of integrated CFPP-PCC model

3.1. Structure of neural network inverse model

In general, a nonlinear autoregressive moving averaging (NARMA) model [53] can be used to describe a multi-input-multi-output (MIMO) system with Eq. (17):

$$y(k) = f(y(k-1),\cdots,y(k-n_y),u(k-\tau),\cdots,u(k-\tau-n_u)) \tag{18}$$

where n_y, n_u are system orders and τ is system time delay. Assume that it exists an inverse model of mentioned MIMO system which can be expressed as Eq. (18)

$$u(k-\tau) = f^{-1}(y(k),y(k-1),\cdots,y(k-n_y),u(k-\tau-1),\cdots,u(k-\tau-n_u)) \tag{19}$$

It can be observed that the inverse control is made available from Eq. (18). $y(k)$ can be replaced by setpoints and the manipulated variables are therefore calculated to make outputs reach target value. A preliminary step for the proposed control scheme is to acquire such an inverse model. Due to its strong learning and approximation ability, artificial neural networks (ANN) is adopted

in this section. The developed inverse model is then used in a neural network inverse control (NNIC) structure. As described in Fig. 6, the manipulated variables can be predicted through neural network inverse model and then used as feed-forward input to control CFPP-PCC system. However, feedback compensation is not concluded in this control structure.

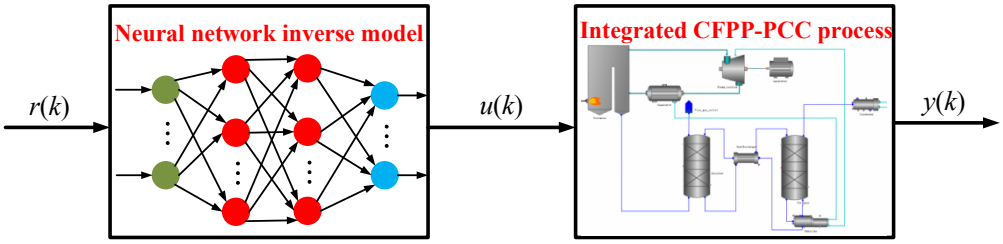

Fig. 6. The NNIC structure for the integrated CFPP-PCC process.

Following the control structures in [40], The integrated CFPP-PCC process can be generally simplified as a 5-inputs-5-outputs system. To acquire the inverse model of mentioned system, a NN structure is presented. As shown in Fig. 7, the input variables of the proposed neural network include: i) the current controlled variables' values from $y_1(k)$ to $y_5(k)$; ii) along with their prior values (assume as first-order system) from $y_1(k\text{-}1)$ to $y_5(k\text{-}1)$ and the manipulated variables' values in the last sampling time from $u_1(k\text{-}1)$ to $u_5(k\text{-}1)$. The outputs of NN inverse model are the predicted values for manipulated variables in current sampling time.

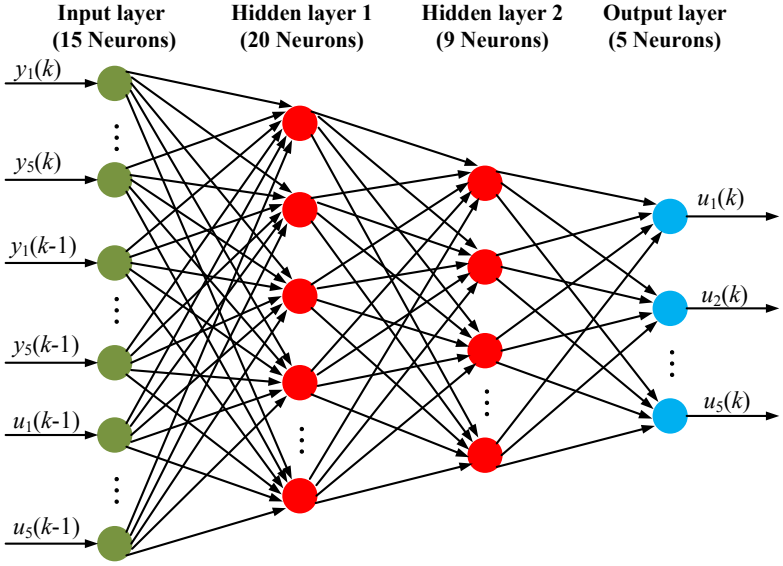

Fig. 7. Structure of neural network inverse model.

3.2. Inverse model training

Back-propagation (BP) neural network is used to approximate the inverse relationship of CFPP-PCC process in this section. BP neural network is a mature and appealing ANN method which has been successfully used in modelling and control of industrial processes [54-55]. As shown in Fig. 7, the BP neural network contains 4 layers. The current and delayed values of controlled variables (CVs) and manipulated variables (MVs) are introduced as inputs. To improve training accuracy, there are 2 hidden layers which contain 20 and 9 neurons respectively.

In order to obtain a neural network model which can fully describe the nonlinear features and dynamic characteristics of mentioned CFPP-PCC system, the training data should be rich enough to contain adequate information over a wide range of operating conditions. In this section, the training data comes from the close-loop simulation of integrated CFPP-PCC model in gCCS environment. 3500 sets of data are collected with a sampling time of 30s. These data include several steady-state conditions from 430MW-540MW and the transient conditions between these load levels. Capture level varies from 50%-90% and reboiler temperature oscillates around the nominal operating points of 392.2K. Fig. 8 displays the prediction of manipulated variables from a NN inverse model. The results show a perfect agreement between the validation data and the prediction results.

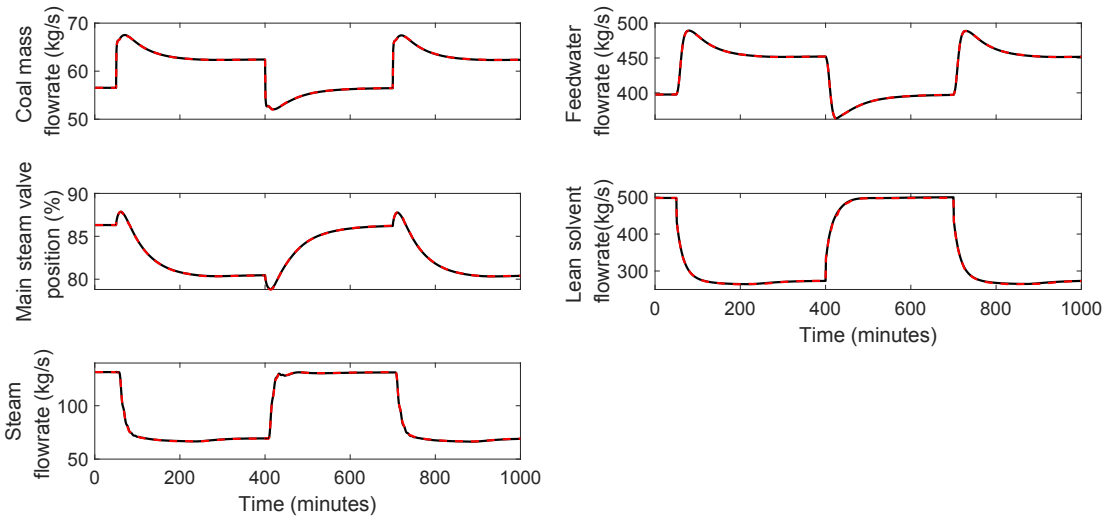

Fig. 8. Training results of NN inverse model (solid in black: measured validation data; dashed in red: inverse model output).

3.3. Improved neural network inverse control scheme

With an accurate NN inverse model, it is able to present an open-loop control configuration without feedback compensation, as shown in Fig. 6. The NNIC is used as a feedforward control. However, the NN inverse model may exhibit steady-state bias and different transient behaviors when it is beyond the working scope. Under this circumstance, an improved NNIC is presented in this section which considers a PID compensator to eliminate steady-state error and guarantee system stability. The manipulated variables $u(k)$ are updated in real-time with a supplementary signal of $u_{PID}(k)$. The combined NNIC and PID compensator is graphically explained in Fig. 9.

To tune parameters of PID compensator, the control loops for PID should be determined. Based on a heuristic approach in Liao et al [56], coal mass flowrate (u_1) is used to control main steam pressure (y_1), feedwater flowrate (u_2) is used to control steam enthalpy in separator (y_2), main steam valve (u_3) is used to control net power output (y_3). In PCC system, capture level (y_4) is controlled by lean solvent flowrate (u_4) and steam flowrate (u_5) is to manipulate reboiler temperature (y_5). In order to dampen the amplification of measurement noise, a PID controller with filtering derivative is adopted. It can be expressed in Eq. (19).

$$\frac{u(s)}{e(s)} = P + \frac{I}{s} + \frac{DNs}{N+s} \tag{20}$$

where e denotes errors between outputs and setpoints, s represents Laplace operator and P, I, D, N are PID controller parameters. In this paper, this structure is applied to both the convention PID controller and the PID compensator.

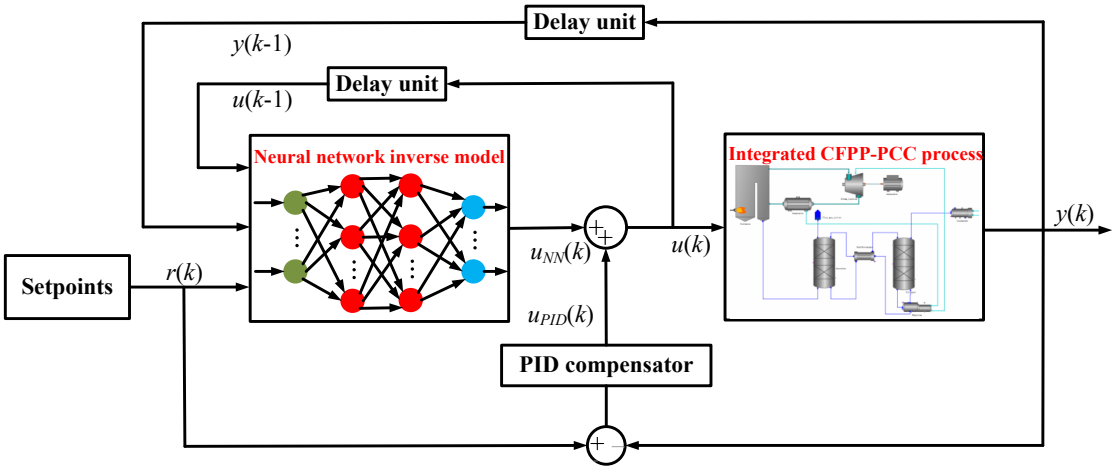

Fig. 9. Schematic topology of proposed neural network inverse control structure.

4. Investigation on open-loop dynamic characteristics

To gain extensive knowledge of underlying physics for the integrated CFPP-PCC process, dynamic behaviors among key variables are investigated through open-loop ramp response tests. As stated in Section 3.3, the coal mass flowrate, feedwater flowrate, main steam valve position, lean solvent flowrate and steam flowrate are taken as the major manipulated variables, while main steam pressure, steam enthalpy in separator, net power output, capture level and reboiler temperature are corresponding controlled variables.

To run simulation, the integrated model is initialized using nominal operating values in Table 3, negative and positive ramp changes (±5% of nominal values) are introduced to coal mass flowrate (u_1), feedwater flowrate (u_2), main steam valve position (u_3), lean solvent flowrate (u_4) and steam draw-off flowrate (u_5) respectively. Changes in these key parameters occur frequently since the power station and PCC process must operate under a wider range of operating conditions with regard to the power and carbon capture demand. The perturbations are gradually introduced to MVs in a period of 5 minutes, after a base condition of 10 minutes. The output responses on main steam pressure (y_1), steam enthalpy in separator (y_2), net power output (y_3), capture level (y_4) and reboiler temperature (y_5) are portrayed in Figs. 10 -14. For a better demonstration, the unaffected CVs are not shown in these figures.

Fig. 10 shows the effect of variation in coal mass flowrate. It is visible that a positive increase in coal mass flowrate contributes an increase in main steam pressure, steam enthalpy and power output. The manipulation on coal mass flowrate is the fundamental method to alter power capacity. The simulation curves exhibit slow dynamics and it takes around 15 minutes to reach new steady state. This time delay mainly results from the pulverizing process. With the increase in coal mass flowrate, the resulting increase in flue gas flowrate will reduce capture level by around 2%. However, the variation of reboiler temperature has only a marginal deviation of approximately 0.00051%. This is possibly because of the large inventory of liquid solvent in PCC process. The fluctuation in flue gas flowrate has only a trivial influence on reboiler temperature.

In Fig. 11, the evaluation on feedwater flowrate are presented. It is observed that the variation in feedwater flowrate doesn't affect downstream PCC process. However, the main steam pressure and power output have a rapid change at the onset of disturbance. For a positive change, an increase in feedwater flowrate means more steam is generated and going through turbine for power generation. The main steam pressure and electricity output has an initial increase. However, the steam temperature at the separator outlet declines gradually since coal flow is unchanged. The volume flowrate and temperature of main steam decrease correspondingly. Main steam pressure and power output reached to its original level. With a continuously reduced separator temperature, the steam enthalpy at separator declines correspondingly.

The third experiment performed aims to test the effect of the main steam valve position. As shown in Fig. 12, the main steam valve has no influence on PCC process. This is based on the assumption that the state (temperature and pressure) of extracted steam is fixed. An increase in valve position can increase electricity output within 2 minutes. This is achieved by using stored energy in the boiler section. With a constant coal mass flowrate, the unit power output will however remain at a lower value after a transient process for around 8 minutes. This proves that main steam valve can be used to control power output to achieve a quick response. In contrast to the variation in feedwater flowrate, an increase in main steam valve results a decrease in the main steam pressure. Due to a fixed coal-feedwater ratio, the steam enthalpy declines at the beginning and then returns to its initial value.

Fig. 13 presents the influence on PCC process in the presence of a ramp change in lean solvent flowrate. It is observed that lean solvent flowrate doesn't affect power plant in an open-loop scenario. A positive increase in lean solvent contributes to an immediate increase in capture level within 15 minutes, followed by a slow evolution towards new steady state (around 100 minutes). The decline is due to the fixed steam flowrate to reboiler, the CO_2 loading of lean solvent is increased which elevates CO_2 equilibrium partial pressure. This will gradually reduce CO_2 absorption level and reboiler temperature.

Reboiler duty is provided by the extracted steam from steam turbine in CFPP. It plays an important role in regeneration process which in turns affects CO_2 capture. The fluctuation in steam draw-off flowrate is of great importance to be investigated. In addition, it has significant impact on net power output. As illustrated in Fig. 14, a positive ramp change in steam flowrate results in an intense decrease in power output. Due to large time constant in PCC process, capture level and reboiler temperature has slow increase. The settling time for capture level and reboiler temperature are around 75-100 minutes. The slow responses in Fig. 13 and Fig.14

prove that PCC process has much larger time constant (75-100 minutes) compared with CFPP (5-30 minutes). In addition, it can be observed that output responses in the presence of positive ramp change resembles with the responses to negative ramp changes in terms of amplitude and settling time. This indicates that CFPP-PCC system has a marginal nonlinearity around the nominal working points. In addition, the dynamic investigation reveals that CFPP and PCC process have strong interactions. It is suggested to consider the integrated CFPP-PCC for controller design instead of considering the standalone PCC process.

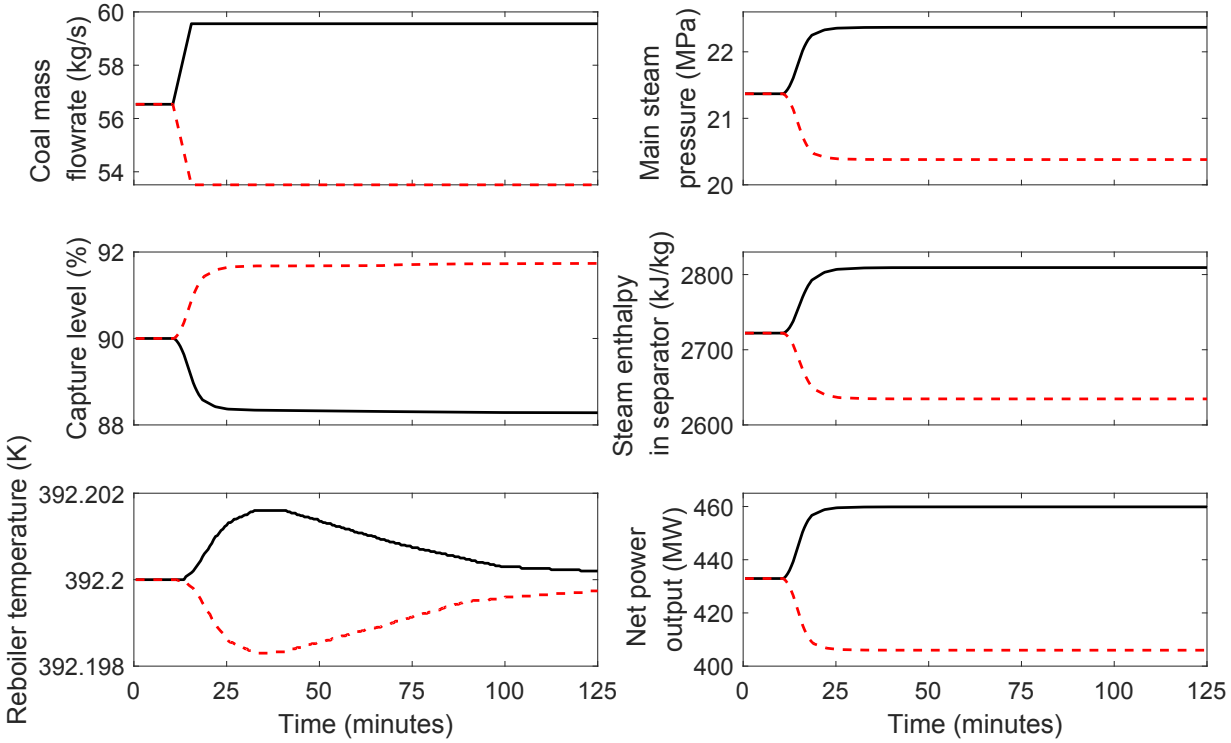

Fig. 10 Responses of CFPP-PCC process with respect to ramp change in coal mass flowrate (Solid in black: +5% ramp change in coal mass flowrate; dashed in red: -5% ramp change in coal mass flowrate)

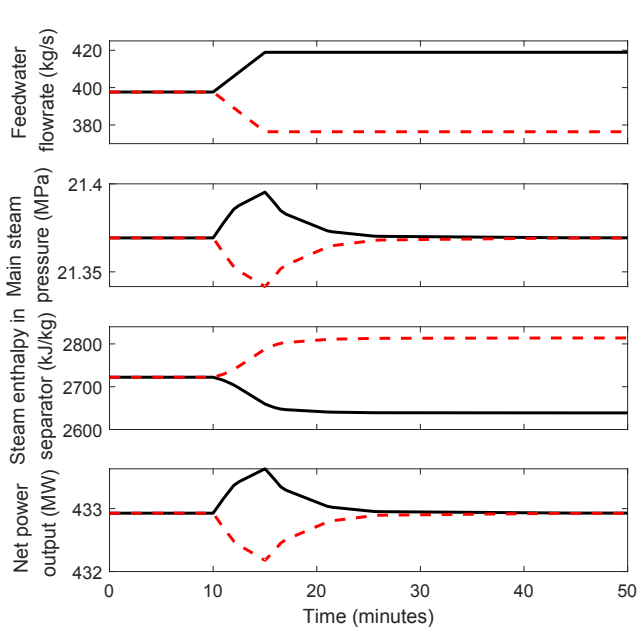

Fig. 11. Responses of CFPP with respect to ramp change in feedwater flowrate (Solid in black: +5% ramp change in feedwater flowrate; dashed in red: -5% ramp change in feedwater flowrate)

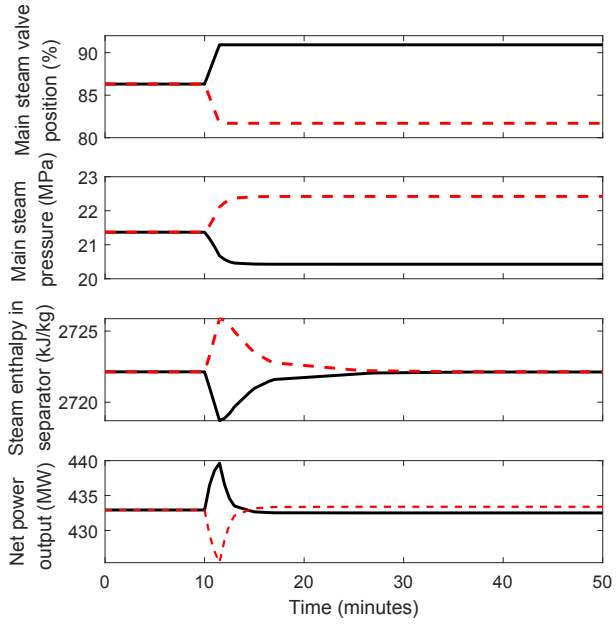

Fig. 12. Responses of CFPP with respect to ramp change in main steam valve position (Solid in black: +5% ramp change in main steam valve position; dashed in red: -5% ramp change in main steam valve position)

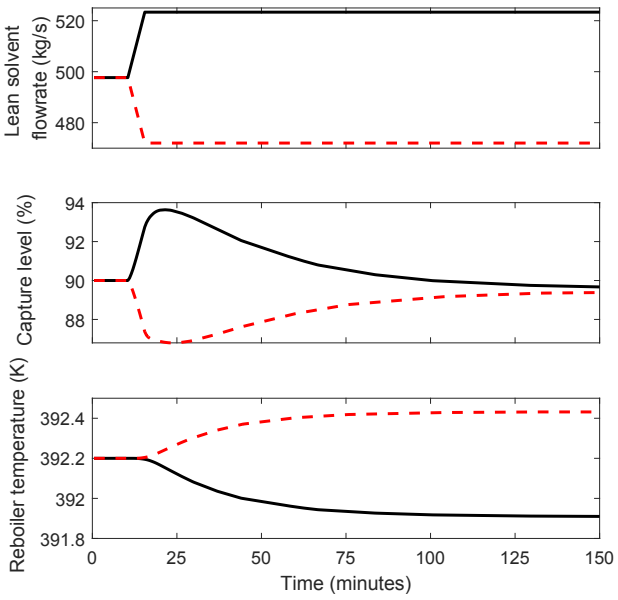

Fig. 13. Responses of PCC process with respect to ramp change in lean solvent flowrate (Solid in black: +5% ramp change in lean solvent flowrate; dashed in red: -5% ramp change in lean solvent flowrate)

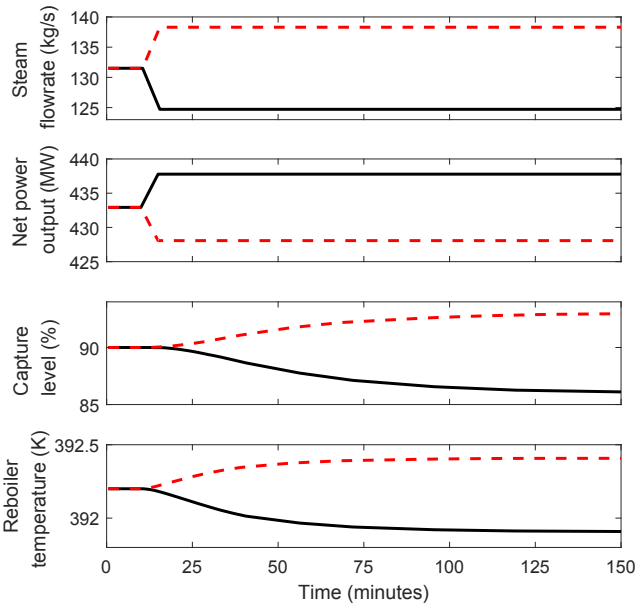

Fig. 14. Responses of CFPP-PCC process with respect to ramp change in steam flowrate (Solid in black: +5% ramp change in steam flowrate; dashed in red: -5% ramp change in steam flowrate)

5. Investigation on operating performance of the CFPP-PCC system under improved NNIC control

In order to evaluate advantages of the improved NNIC, dynamic simulations of the integrated CFPP-PCC process are carried out under two scenarios: i) step change in net power output setpoint and ii) step change in capture level setpoint. These two scenarios are frequent cases encountered in the daily operation of a CFPP-PCC process. On the one hand, CFPP needs to alter power setpoint in order to adapt with the variation in grid demand. On the other hand, it is necessary to change capture level setpoint to balance the operation between CFPP and PCC at different electricity price conditions. At peak electricity price, it is suggested to lower capture level setpoint to let more steam for power generation. At low electricity price, more steam should be extracted to increase carbon capture level so that PCC process can satisfy the environmental demand. To this regard, it is of importance to investigate the controllability of proposed controller in these two cases.

To highlight the potential of improved NNIC, a conventional PID control structure in [17] and standalone NNIC (as shown in Fig. 6) are adopted for comparison. Insight from this comparison will help to investigate the similarities and differences in the operation using different controllers (e.g. improved NNIC, convention PID and standalone NNIC). A Ziegler-Nichols method is adopted to tune PID parameters [57]. The parameters used in conventional PID controllers are listed in Table 4.

Table 4. Conventional PID controller parameters

Control loops	P	I	D	N
Main steam pressure control loop	2.0446	0.046	5.4559	0.0441
Steam enthalpy control loop	-0.017	-0.00623	0.001	0.321
Net power output control loop	0.0001169	4.261e-06	0	0
Capture level control loop	25.321	1.7253	0	0
Reboiler temperature control loop	105.301	1.2125	2.21	0.125

5.1. Case study 1 – step change in power output setpoint

Coal-fired power units must be operated flexibly to accommodate the large shares of intermittent energy sources like solar and wind energy. With frequent power load changes, significant effects would be incurred in the integrated CFPP-PCC system. System performances in the presence of multi-load changes are investigated in this section. The integrate system is initially operated under

nominal points as listed in Table 3. After a base condition of 10 minutes, setpoints of the main steam pressure, steam enthalpy and power output are stepped up from 21.3693 MPa, 2722.1325 kJ/kg, 432.927MW to 24.8430 MPa, 2674.4886 kJ/kg and 552.790 MW respectively. At t=110 minutes, the setpoints of above variables change to 24.01 MPa, 2702.4781 kJ/kg and 506.896 MW. The second part of simulation lasts for 100 minutes. Capture level and reboiler temperature setpoints are fixed at 90% and 392.2 K for the whole simulation. In this scenario, the simulation is within the working range of NN inverse model. This means that NN inverse model can give accurate prediction of the manipulated variables. Simulation results are shown in Figs. 15-18.

Fig. 15 shows the responses of CFPP controlled variables. It can be observed that improved NNIC is able to maintain a tight control and attain the best control performances. With a precise prediction in NN inverse model, the standalone NNIC can also attain satisfactory performances with zero steady-state bias. Only trivial difference in system performances are observed for these two control schemes. When the setpoints change, NN inverse model can calculate desired output and then assign these values to input channels, driving the controlled variables to quickly follow the references. Main steam pressure and net power output can reach steady-state within 10 minutes while conventional PID takes more than 25 minutes to stabilize.

Besides, difference in the response of steam enthalpy is noteworthy. It can be noticed that steam enthalpy using PID controllers has an initial increase at the onset of simulation, while standalone NNIC and improved NNIC result in a slight decrease before finalized to steady state. This can be explained by the manipulation on input variables. As presented in Fig. 16, coal mass flowrate has a quick increase rate compared with feedwater flowrate in a PID control structure (solid line in blue). At beginning, the rising coal flowrate will generate more steam in separator and therefore increase steam temperature and steam enthalpy. With the continuous increase in feedwater flowrate, the temperature in separator will decline and thus decrease the steam enthalpy. On the contrary, immediate manipulations on coal mass flowrate and feedwater flowrate are introduced for NNIC. It will have a significant influence on separator temperature and therefore decrease steam enthalpy to a lower value. This simulation proves that feedwater flowrate is the dominant factor influencing steam enthalpy.

Fig. 17 shows the simulation results of the PCC process. In both standalone NNIC and improved NNIC structure, capture level has a satisfactory control performance and can be settle down within 40 minutes. It exhibits much lower oscillation compared with PID controllers. An opposite response tendency for capture level can be observed. This is similar with the variation in the steam enthalpy at separator outlet. As shown in Fig. 18, NNIC has fast operation on lean solvent flowrate and steam flowrate (line in red and green) and this will lead to an initial increase in capture level. However, conventional PID controllers is an error-based feedback controller. The large time constant leads to a slow manipulation on lean solvent and steam flowrates. As indicated in Section 4, power unit exhibits a much lower time constant. The operation in coal mass flowrate (Fig. 16: solid in blue) therefore has a quick rise. The resulting increase in flue gas flowrate will reduce capture level at the beginning.

However, the tight control in capture level is at the cost of reboiler temperature. It exhibits larger oscillation (0.05 K) in both two NNIC structures compared with PID controllers (0.01 K). This is due to the fast manipulation on lean solvent flowrate and steam flowrate. This will put challenge on the tight control for reboiler temperature.

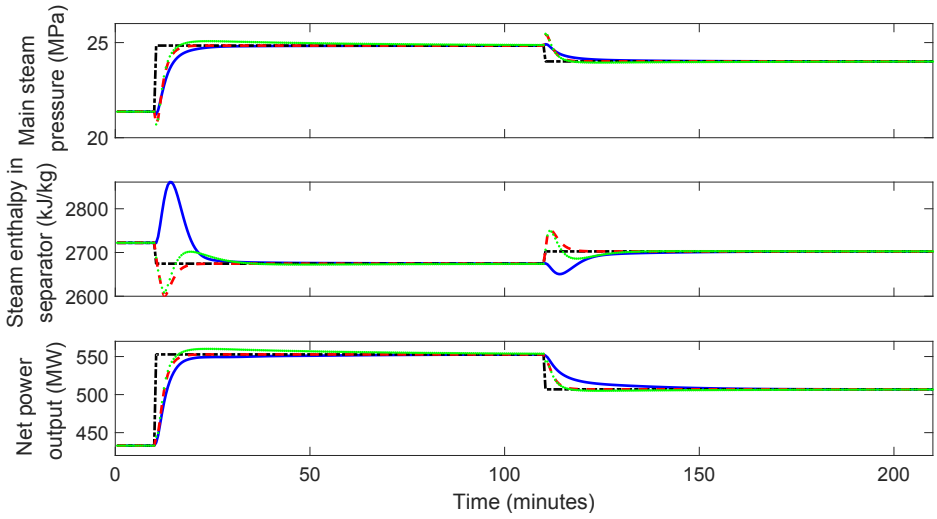

Fig. 15. Performance of CFPP controlled variables in Case 1 (dash-doted in black: reference; solid in blue: conventional PID controllers; dashed in red: standalone NNIC; doted in green: improved NNIC)

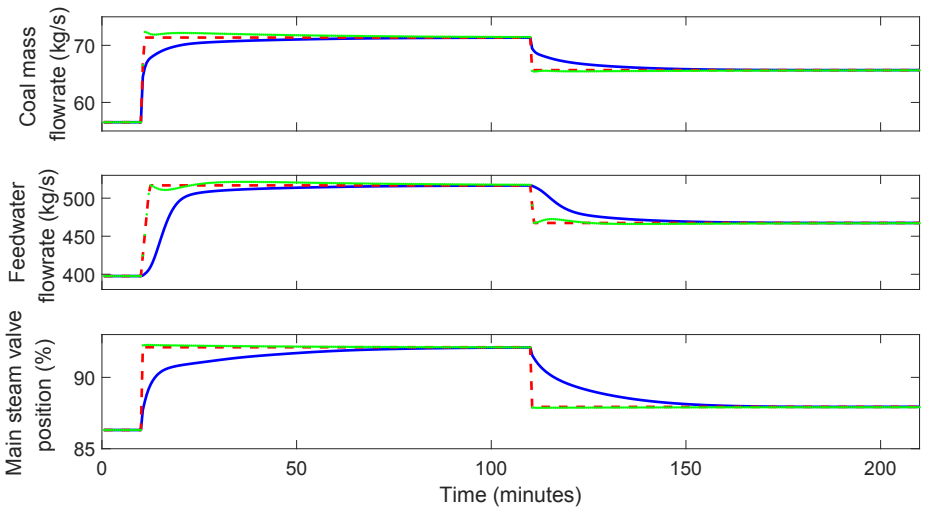

Fig. 16. Performance of CFPP manipulated variables in Case 1 (solid in blue: conventional PID controllers; dashed in red: standalone NNIC; doted in green: improved NNIC)

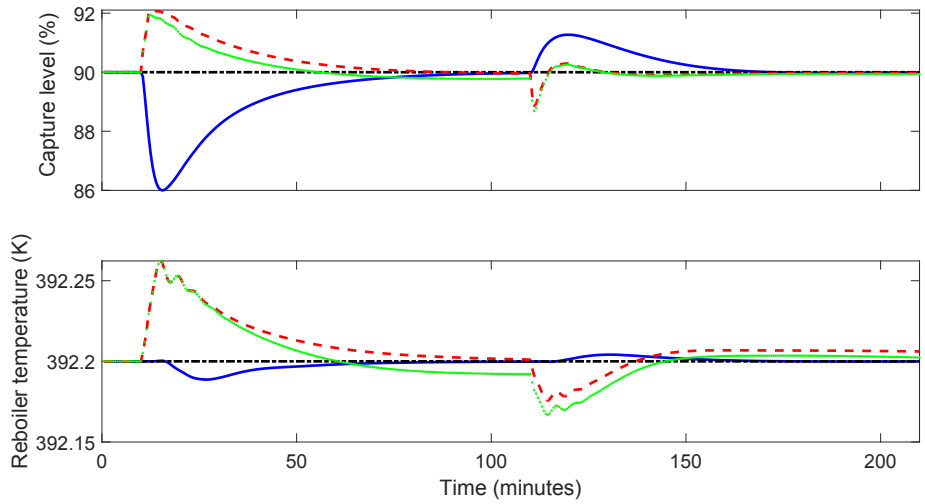

Fig. 17. Performance of PCC controlled variables in Case 1 (dash-doted in black: reference; solid in blue: conventional PID controllers; dashed in red: standalone NNIC; doted in green: improved NNIC)

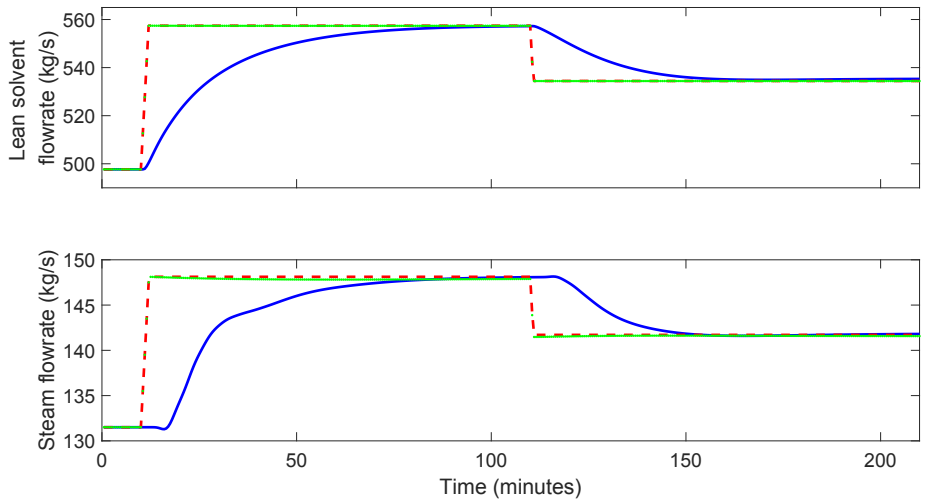

Fig. 18. Performance of PCC manipulated variables in Case 1 (solid in blue: conventional PID controllers; dashed in red: standalone NNIC; doted in green: improved NNIC)

5.2. Case study 2 – step change in capture level setpoint

This case simulates the change in CO_2 capture level setpoint from the base case value 90% to 50% and then to 95%. Power plant output targets and reboiler temperature setpoint are maintained during the whole simulation. As stated in Section 3.2, the training data for NN inverse model ranges from 430MW to 530MW and the capture level varies from 50% to 90%. The NN inverse model is proven to give quantitative agreement between the predicted manipulated data and the actual values within working area, as shown in Fig. 8. This reveals that the NN inverse model is able to precisely predict manipulated variables at 50% capture level and may fail to work at 95% capture level. Wu et al [2] and Liao et al [5] report significant nonlinear features of PCC process between 90% capture level and 95% capture level. The strong nonlinearity will even deteriorate the estimation of NN inverse model. In this section, the integrated CFPP-PCC system is operated at nominal conditions for a base period of 10 minutes. The whole plant is simulated for 125 minutes at the capture level setpoint of 50% and then simulated for another 125 minutes at the capture level setpoint of 95%. Responses of integrated system are expressed in Figs. 19-22.

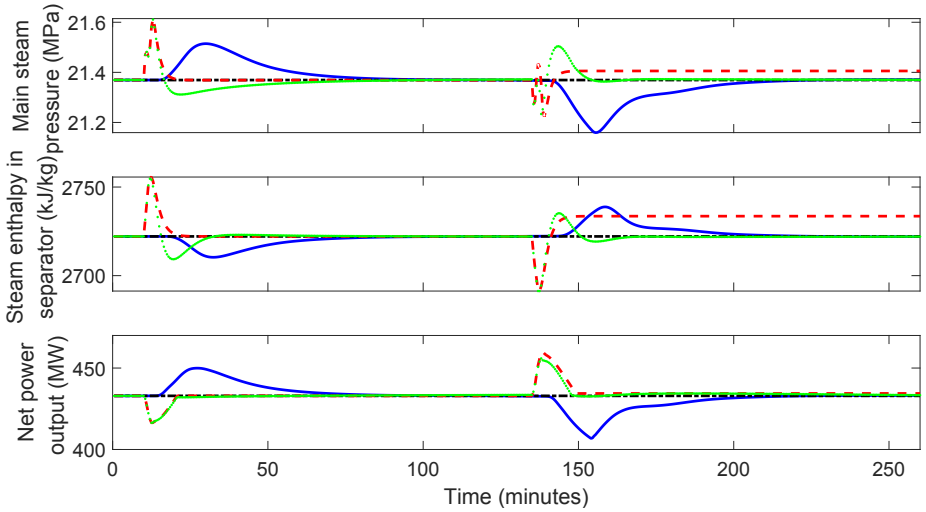

Fig. 19. Performance of CFPP controlled variables in Case 2 (dash-doted in black: reference; solid in blue: conventional PID controllers; dashed in red: standalone NNIC; doted in green: improved NNIC)

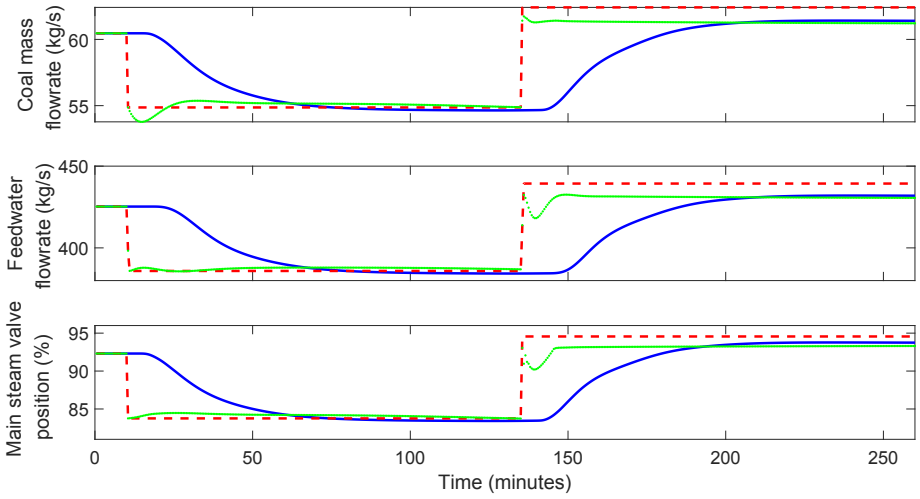

Fig. 20. Performance of CFPP manipulated variables in Case 2 (solid in blue: conventional PID controllers; dashed in red: standalone NNIC; doted in green: improved NNIC)

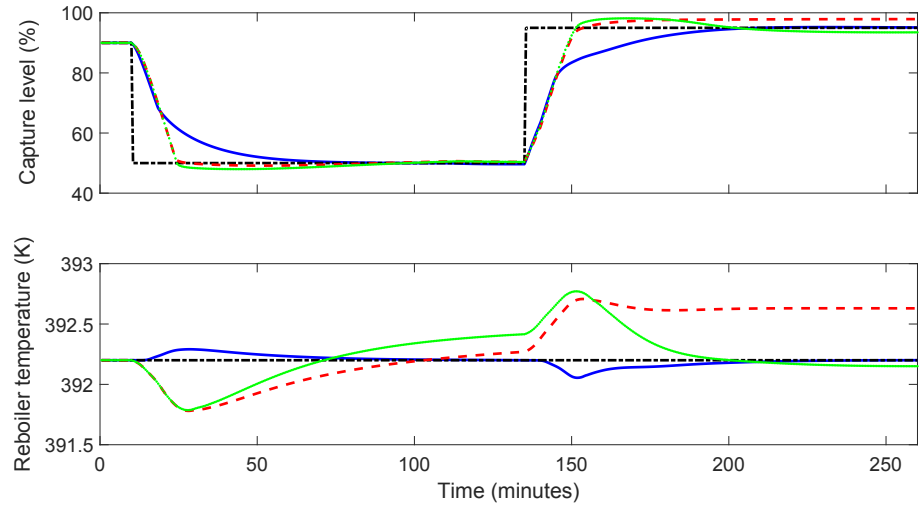

Fig. 21. Performance of PCC controlled variables in Case 2 (dash-doted in black: reference; solid in blue: conventional PID controllers; dashed in red: standalone NNIC; doted in green: improved NNIC)

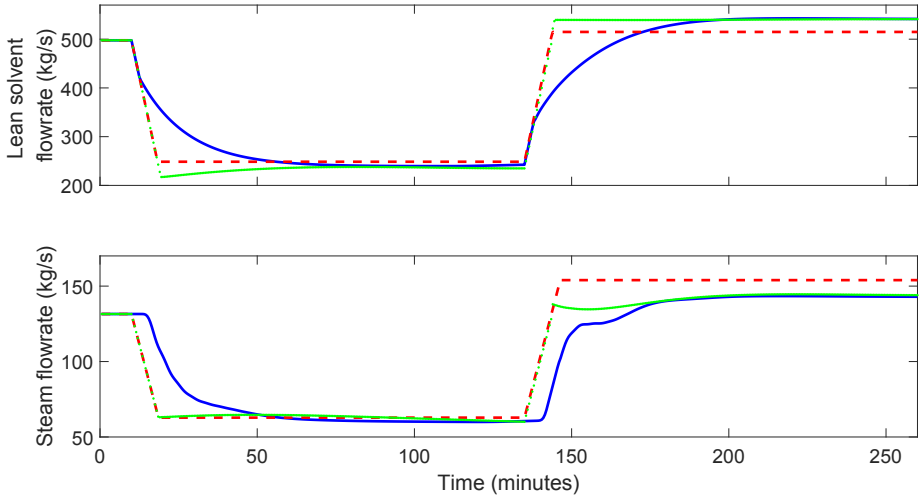

Fig. 22. Performance of PCC manipulated variables in Case 2 (solid in blue: conventional PID controllers; dashed in red: standalone NNIC; doted in green: improved NNIC)

From Fig. 19 and Fig. 21, it can be observed that both the standalone NNIC and the improved NNIC are able to achieve satisfactory control performances at the first part of simulation (capture level setpoint at 50%). Capture level can quickly reach the new steady state (10 minutes) with less fluctuation compared to that observed in convention PID controllers (55 minutes). This is because of the tight control on manipulated variables as shown in Fig.20 and Fig. 22. NN inverse model can provide with satisfactory estimation of manipulated variables. Nevertheless, an obvious time delay of 6 minutes is visible in the manipulations on coal mass flowrate, feedwater flowrate and main steam valve position in PID control structure (Fig. 20: solid in blue), which differs from the operation in Case 1. This is due to the large time constant and time delay in PCC process. In Case 2, variation in capture level setpoint leads to a change in lean solvent flowrate and this will take approximately 5 minutes influencing reboiler temperature. The steam flowrate will therefore change and affect the upstream CFPP. To this end, manipulated variables takes longer time (6 minutes) to adapt with the variation in capture level setpoint. In contrast, Case 1 simulates the performances with a step change in power load demand and this will make an immediate manipulation at the start of simulation.

In the second part of simulation (capture level setpoint at 95%), Fig. 19 and Fig. 21 outline an obvious deviation in output results in the standalone NNIC compared with PID controllers and the improved NNIC. The improved NNIC can effectively remove steady-state bias with the additional manipulation from PID compensator. With the NN inverse model providing feed-forward signal, it is capable of achieving better control performances in respect to net power electricity and capture level.

6. Conclusion

In this paper, a dynamic model of large-scale super-critical CFPP integrated with solvent-based PCC process is presented in gCCS software. Open-loop ramp response tests are carried out to investigate the dynamic characteristics of the CFPP-PCC process. It is found that the CFPP and the PCC process have strong interactions. Flue gas and extracted steam to reboiler are proven to be the key connections between two sub-systems. It is therefore suggested to consider the integrated CFPP-PCC for controller design instead of considering the standalone CFPP and PCC processes separately. In addition, PCC process exhibits large time constant (75-100 minutes) which is far more than CFPP (5-30 minutes). The strong interactions and the large time constant in the CFPP-PCC process make it difficult for decentralized PID controller to achieve satisfactory control performance. To solve these problems and to operate the integrated CFPP-PCC system flexibly, an advanced control structure which utilizes the combination of NNIC and conventional PID is developed. The NNIC considers the coupling effects of different variables and can achieve a feed-forward control with variation in setpoints, while the PID can guarantee an offset-free tracking of the control system in the presence of modelling mismatches and plant behavior change. The resulting improved NNIC has shown to operate the CFPP-PCC system reaching setpoints quickly with zero steady-state bias at all scenarios.

Acknowledgements

The authors would like to acknowledge the National Natural Science Foundation of China (NSFC) under Grants 51976030 and 51936003, National Key Research and Development Project under Grand 2018YFB1502904, Natural Science Foundation of Jiangsu Province for Outstanding Young Scholars under Grant BK20190063, the Royal Society - Sino British Fellowship Trust International Fellowship and Excellent Young Scholars support program of Southeast University for funding this work.

References

[1] International Energy Agency (IEA), 2018. World: Electricity and Heat for 2015. OECD/IEA.

[2] Bui M, Gunawan I, Verheyen V, Feron P, Meuleman E, Adeloju S. Dynamic modelling and optimisation of flexible operation in post-combustion CO_2 capture plants-A review. Computers & Chemical Engineering 2016; 61: 245-265.

[3] Wu X, Wang M, Liao P, Shen J, Li Y. Solvent-based post-combustion CO_2 capture for power plants: A critical review and perspective on dynamic modelling, system identification, process control and flexible operation. Applied Energy, 2020, 257: 113941.

[4] Wu X, Shen J, Li Y, Wang M, Lawal A, Lee KY. Nonlinear dynamic analysis and control design of a solvent-based post-combustion CO2 capture process. Computers & Chemical Engineering 2018; 115: 397-406.

[5] Liao P, Wu X, Li Y, Wang M, Shen J, Lawal A, Xu C. Application of piece-wise linear system identification to solvent-based post-combustion carbon capture. Fuel 2018; 234: 526-537.

[6] Wu X, Shen J, Li Y, Wang M, Lawal A. Flexible operation of post-combustion solvent-based carbon capture for coal-fired power plants using multi-model predictive control: A simulation study. Fuel 2018; 220: 931-941.

[7] Gaspar J, Fosbøl PL. Simulation and multivariable optimization of post-combustion capture using piperazine. International Journal of Greenhouse Gas Control 2016; 49: 227-238.

[8] Zhang W, Chen J, Luo X, Wang M. Modelling and process analysis of post-combustion carbon capture with the blend of 2-amino-2-methyl-1-propanol and piperazine. International Journal of Greenhouse Gas Control 2017; 63: 37-46.

[9] Schach MO, Schneider R, Schramm H, Repke JU. Techno-economic analysis of post-combustion processes for the capture of carbon dioxide from power plant flue gas. Industrial & Engineering Chemistry Research 2010; 49(5): 2363-2370.

[10] Mac Dowell N, Shah N. The multi-period optimisation of an amine-based CO_2 capture process integrated with a super-critical coal-fired power station for flexible operation. Computers & Chemical Engineering 2015; 74: 169-183.

[11] Lawal A, Wang M, Stephenson P, Koumpouras G, Yeung H. Dynamic modelling and analysis of post-combustion CO_2 chemical absorption process for coal-fired power plants. Fuel 2010; 89: 2791-2801.

[12] Mac Dowell N, Samsatli NJ, Shah N. Dynamic modelling and analysis of an amine-based post-combustion CO_2 capture absorption column. International Journal of Greenhouse Gas Control 2013; 12: 247-258.

[13] Bui M, Tait P, Lucquiaud M, Mac Dowell N. Dynamic operation and modelling of amine-based CO_2 capture at pilot scale. International Journal of Greenhouse Gas Control 2018; 79: 134-153.

[14] Van De Haar A, Trapp C, Wellner K, Kler R, Schmitz G, Colonna, P. Dynamics of post-combustion CO_2 capture plants: Modeling, validation, and case study. Industrial & engineering chemistry research 2017; 56(7): 1810-1822.

[15] Pintola T, Tontiwachwuthikul P, Meisen A. Simulation of pilot plant and industrial CO_2-MEA absorbers. Gas separation & purification 1993; 7(1): 47-52.

[16] Alatiqi I, Sabri M F, Bouhamra W, Alper E. Steady-state rate-based modelling for CO_2 amine absorption-desorption systems[J]. Gas separation & purification 1994; 8(1): 3-11.

[17] Lawal A, Wang M, Stephenson P, Obi O. Demonstrating full-scale post-combustion CO_2 capture for coal-fired power plants through dynamic modelling and simulation. Fuel 2012; 101: 115-128.

[18] Léonard G, Cabeza Mogador B, Belletante S, Heyen G. Dynamic modelling and control of a pilot plant for post-combustion CO_2 capture. Computer Aided Chemical Engineering 2013; 31: 451-456.

[19] Prölß K, Tummescheit H, Velut S, Åkesson J. Dynamic model of a post-combustion absorption unit for use in a non-linear model predictive control scheme. Energy Procedia 2011; 4: 2620-2627.

[20] Åkesson J, Laird CD, Lavedan G, Prölß K, Tummescheit H, Velut S, Zhu Y. Nonlinear Model Predictive Control of a CO_2 Post-Combustion Absorption Unit. Chemical Engineering & Technology 2012; 35(3): 445-454.

[21] Arce A, Mac Dowell N, Shah N, Vega LF. Flexible operation of solvent regeneration systems for CO_2 capture processes using advanced control techniques: Towards operational cost minimization. International Journal of Greenhouse Gas Control 2012; 11: 236-250.

[22] Gaspar J, Cormos A M. Dynamic modeling and absorption capacity assessment of CO_2 capture process. International Journal of Greenhouse Gas Control 2012; 8: 45-55.

[23] Lin YJ, Chang CC, Wong DSH, Jang SS, Ou JJ. Control strategies for flexible operation of power plant with CO_2 capture plant. AIChE Journal 2012; 58: 2697-2704.

[24] Lin YJ, Pan TH, Wong DSH, Jang SS, Chi YW, Yeh CH. Plantwide control of CO_2 capture by absorption and stripping using mono-ethanolamine solution. Industrial & Engineering Chemistry Research 2010; 50: 1338-1345.

[25] Nittaya T, Douglas PL, Croiset E, Luis A, Sandoval R. Dynamic modelling and control of MEA absorption processes for CO_2 capture from power plants. Fuel 2014; 116: 672-691.

[26] Mechleri E, Lawal A, Ramos A, Davison J, Mac Dowell N. Process control strategies for flexible operation of post-combustion CO_2 capture plants. International Journal of Greenhouse Gas Control 2017; 57: 14-25.

[27] Harun N. Dynamic simulation of MEA absorption process for CO_2 capture from power plant. PhD thesis, University of Waterloo; 2012.

[28] Sahraei MH, Ricardez-Sandoval LA. Controllability and optimal scheduling of a CO_2 capture plant using model predictive control. International Journal of Greenhouse Gas Control 2014; 30: 58-71.

[29] He Z, Sahraei MH, Ricardez-Sandoval LA. Flexible operation and simultaneous scheduling and control of a CO_2 capture plant using model predictive control. International Journal of Greenhouse Gas Control 2016; 48: 300-311.

[30] Li Z, Ding Z, Wang M, Oko E. Model-free adaptive control for MEA-based post-combustion carbon capture processes. Fuel 2018; 224: 637-643.

[31] Liao P, Li Y, Wang M, Wu X, Shen J. Review of dynamic modelling, system identification and control scheme in solvent-based post-combustion carbon capture process. Energy Procedia 2017; 142: 3505-3510.

[32] Wang L. Model predictive control system design and implementation using MATLAB. Springer Science & Business Media, 2009.

[33] Borhani TN, Oko E, Wang M. Process modelling and analysis of intensified CO_2 capture using monoethanolamine (MEA) in rotating packed bed absorber. Journal of Cleaner Production 2018; 204: 1124-1142.

[34] Cifre PG, Brechtel K, Hoch S, Garcia H, Asprion N, Hasse H, Scheffknecht G. Integration of a chemical process model in a power plant modelling tool for the simulation of an amine-based CO_2 scrubber. Fuel 2009; 88(12): 2481-2488.

[35] Sanpasertparnich T, Idem R, Bolea I, deMontigny D, Tontiwachwuthikul P. Integration of post-combustion capture and storage into a pulverized coal-fired power plant. International Journal of Greenhouse Gas Control 2010; 4(3): 499-510.

[36] Olaleye AK, Wang M, Kelsall G. Steady state simulation and exergy analysis of supercritical coal-fired power plant with CO_2 capture. Fuel 2015; 151: 57-72.

[37] Zhai R, Yu H, Chen Y, Li K, Yang Y. Integration of the 660 MW supercritical steam cycle with the NH3-based CO_2 capture process: System integration mechanism and general correlation of energy penalty. International Journal of Greenhouse Gas Control 2018; 72: 117-129.

[38] Oh SY, Yun S, Kim JK. Process integration and design for maximizing energy efficiency of a coal-fired power plant integrated with amine-based CO_2 capture process. Applied Energy 2018; 216: 311-322.

[39] Olaleye AK, Oko E, Wang M, et al. Dynamic modelling and analysis of supercritical coal-fired power plant integrated with post-combustion CO_2 capture. Clean Coal Technology and Sustainable Development. Springer, Singapore 2016: 359-363.

[40] Wu X, Wang M, Shen J, Li Y, Lawal A, Lee KY. Flexible operation of coal fired power plant integrated with post combustion CO_2 capture using model predictive control. International Journal of Greenhouse Gas Control 2019; 82: 138-151.

[41] Wu X, Wang M, Shen J, Li Y, Lawal A, Lee KY. Reinforced coordinated control of coal-fired power plant retrofitted with solvent based CO_2 capture using model predictive controls. Applied Energy 2019; 238: 495-515.

[42] Awad T, Elgohary MA, Mohamed TE. Ship roll damping via direct inverse neural network control system. Alexandria engineering journal, 2018, 57(4): 2951-2960.

[43] Ramli NM, Hussain MA, Jan BM. Multivariable control of a debutanizer column using equation based artificial neural network model inverse control strategies. Neurocomputing, 2016, 194: 135-150.

[44] Lee KY, Ma L, Boo CJ, Jung WH, Kim SH. Inverse dynamic neuro-controller for superheater steam temperature control of a large-scale ultra-supercritical (USC) boiler unit. IFAC Proceedings Volumes, 2009, 42(9): 107-112.

[45] Fan H, Zhang YF, Su ZG, Wang B. A dynamic mathematical model of an ultra-supercritical coal fired once-through boiler-turbine unit. Applied Energy 2017; 189: 654-666.

[46] Zhuo X, Zhou H, Yang C, Tang H. Dynamic Modelling for a Coal-fired Drum Boiler Power Unit and Validation Through Using Actual Plant Data. Proceedings of the CSEE, 2008, 17: 006.

[47] Liu JZ, Yan S, Zeng DL, Hu Y, Lv Y. A dynamic model used for controller design of a coal fired once-through boiler-turbine unit. Energy 2015; 93: 2069-2078.

[48] Zhao H, Shen J, Li Y, Bentsman J. Coal-fired utility boiler modelling for advanced economical low-NOx combustion controller design. Control Engineering Practice 2017; 58: 127-141.

[49] Eberhart RC, Shi Y. Comparison between genetic algorithms and particle swarm optimization. International conference on evolutionary programming. Springer, Berlin, Heidelberg 1998: 611-616.

[50] Li L, Liu WX, Cartes DA. Particle swarm optimization-based parameter identification applied to permanent magnet synchronous motors. Engineering Applications of Artificial Intelligence 2008: 1092-1100.

[51] Sinnott RK. Chemical engineering design. 4th ed. Oxford, UK: Butterworth-Heinemann; 2005.

[52] Lawal A. Study of post-combustion CO2 capture for coal-fired power plant through modelling and simulation. Cranfield University, 2010.

[53] Chon KH, Cohen RJ. Linear and nonlinear ARMA model parameter estimation using an artificial neural network. IEEE Transactions on Biomedical Engineering 1997; 44(3): 168-174.

[54] Liang W, Wang G, Ning X, Zhang J, Li Y, Jiang C, Zhang N. Application of BP neural network to the prediction of coal ash melting characteristic temperature. Fuel, 2020, 260: 116324.

[55] Yan C, Li M, Liu W, Qi M. Improved adaptive genetic algorithm for the vehicle Insurance Fraud Identification Model based on a BP Neural Network. Theoretical Computer Science, 2019.

[56] Liao P, Wu X, Li Y, Wang M, Shen J, Sun B, Pan L. Flexible operation of coal-fired power plant integrated with post-combustion CO_2 capture. Energy Procedia 2019; 158: 4810-4815.

[57] Valério D, Da Costa JS. Tuning of fractional PID controllers with Ziegler-Nichols-type rules. Signal processing, 2006, 86(10): 2771-2784.